Acta Geotechnica
https://doi.org/10.1007/s11440-023-02118-6

RESEARCH PAPER

Pullout resistance of biomimetic root-inspired foundation systems

Thibaut Houette[1] · Meron Dibia[1] · Nariman Mahabadi[2] · Hunter King[3,4]

Received: 17 February 2023 / Accepted: 24 October 2023

Abstract
Deep foundation and anchorage systems are often comprised of simple linear elements, limited by design, materials and techniques employed to build them. Their stability is attained by transferring structural loads to deeper, more stable soil layers across a larger area, reducing potential for excessive settlement and providing resistance against lateral forces from external factors including wind and earthquakes. In comparison, root systems distribute loads to a large volume of soil through a branched morphology of semiflexible elements. Roots also penetrate soil media, reduce erosion, create habitats, and exchange, store and transport resources, while continuously sensing and adapting to environmental conditions. Insights from their integration of multifunctionality can be transferred to civil engineering through biomimicry. As a first step toward designing root-inspired foundations, the effects of various morphological traits (laterals' length, number of nodes, number of laterals, branching angle and laterals' cross section) on foundation performance are evaluated through vertical pullout tests. Out of the model properties, general trends were observed, including the positive correlation between models' surface area and maximum force reached. Yet, due to complex interactions between the model and granular media, no model property fully explained differences in pullout resistance of all models. The effects of each root trait on pullout resistance were analyzed separately, which can serve to adapt the design of root-inspired foundations and exploit granular physics principles. Potential reasons for surprising and counterintuitive results are also presented. Further studies could evaluate the assumptions given as potential explanations of these results by studying identified counterintuitive scenarios.

Keywords Biomimicry · Bio-inspired geotechnics · Biological roots · Branched foundations · Civil engineering · Pullout resistance

1 Introduction

The continuous expansion of the built environment affects numerous ecosystem services (e.g., regulating floods, limiting erosion, providing natural habitat for biodiversity and supporting nutrient cycling) previously provided by natural environments [23, 34, 45]. Urban design has an obligation to supply or replace such services to limit the effects on global resource cycles. Current deep foundations are mostly simple monofunctional systems designed as linear elements of constant cross section due to limited insertion techniques and material availability [9]. Structural stability is achieved by transferring the structural loads to deeper, more stable layers of soils or rock, therefore distributing the loads over a larger area, increasing the bearing capacity of soil, minimizing the risk of excessive settlement and providing resistance to lateral forces that can arise from wind, earthquake or other external factors [15, 36]. The low surface area of foundation systems is compensated with a need for an increased soil stability achieved through depth or compaction which reduces soil permeability and water infiltration, leading to increased flooding severity in cities and lack of aquifer recharge [2, 77]. Compaction also limits the development of green corridors throughout built environments [75]. Heavy construction methods are employed to reach deeper more stable soil layers, which generate

✉ Thibaut Houette
thibaut.houette@gmail.com

1 Department of Biology, The University of Akron, Akron, OH, USA

2 Department of Civil Engineering, The University of Akron, Akron, OH, USA

3 Center for Computational and Integrative Biology, Rutgers University-Camden, Camden, NJ, USA

4 Department of Physics, Rutgers University-Camden, Camden, NJ, USA

Published online: 24 November 2023

environmental disturbance (i.e., both natural and built) along with increased resource usage (i.e., time, materials, energy, individuals and funding). High soil heterogeneity coupled with a lack of sensing, accessibility and adaptation induce high factors of safety. For instance, current techniques to produce frictional piles (e.g., auger cast in place foundation piles) generate friction coefficients of low precision, necessitating even more cautious strategies and over-engineering. The end of deep foundations' life cycle is usually neglected by leaving them in the ground without being able to reuse, recycle nor biologically decompose them, leading to soil congestion. Most problems presented stem from traditional design principles, insertion techniques and materials, which limit foundation systems to mostly heavy structures of simple vertical pile morphology [30]. The bearing area of such morphology is very low, and most of the materials interact with surrounding soil media through friction. Traditional principles need to be challenged to find inspiration into other possibilities to perform structural anchorage through innovative design morphologies, directional soil penetration and more tunable material properties.

On the other end, biological root systems anchor the tree by transmitting loads to a large volume of soil through a spatial distribution of semiflexible branching structures. To maximize root/soil mechanical and chemical interaction, roots form hierarchical mesh morphologies ranging from meters (i.e., large roots) down to micrometers (i.e., root hairs) and even beyond when considering further mechanisms such as mucilage [72]. Root systems also serve to keep the soil in the form of a coherent block, or root/soil plate [12], by providing anchor points for the self-organizing, sparse, load bearing structures of interparticle contacts known as force chains [43]. The formation and disruption of force chain networks determine the phase behavior of the granular material [51], resisting deformation as a solid or allowing flow as a fluid, respectively. The bulk weight of these granular particles and loads applied to them are not evenly distributed but concentrated on specific areas following the force chain network that bear the bulk of the stress in the arrangement. In addition to structural support, roots perform numerous functions (both actively and passively), including continuous sensing, adaptation to physical and chemical properties of soil, soil exploration, resource uptake, storage and discharge, erosion prevention and habitat creation [41, 57, 58]. Complex root anatomy allows this integration of multifunctionality within one hierarchical structure. Studying root systems for inspiration can lead to multifunctional building foundations with adaptable morphologies.

The biomimicry approach can be employed to transfer biological strategies observed in tree roots toward the design of multifunctional sustainable foundation systems [9, 10, 16, 30, 46, 47, 67]. Literature reviews of root anchorage, root erosion prevention and foundation design were completed and published in [67]. Performance requirements and environmental constraints of foundations differ from those of root systems [16]. Some functions of root systems do not always make sense to transfer to foundations. For example, a tree grows from a seed through a series of life stages, while a foundation can be designed and built from scratch, far away from its final application setting. Therefore, the goal is not to create foundation systems that look like root systems but rather to abstract and transfer strategies (i.e., including morphology and mechanisms) that allow root systems to perform specific functions toward geotechnical applications. A variety of root traits have been identified as promising for the design of root-inspired anchorage due to their ability to control the system's stiffness, peak strength and ductility: material stiffness and strength, root diameter, taper, orientation and branching pattern [10]. Other principles of interest include surface area-to-volume ratio, porosity, cross section, asymmetry, curvature, friction coefficient and tip morphology [38, 67]. Depending on the loading scenario of a design project, different sets of root traits can be analyzed. Multiple traits and concepts are likely to be relevant for a range of loading scenarios as they share similar local biomechanical behaviors [9].

Resistance to uprooting is critical in biological roots to resist grazing [28, 60] and more complex loading scenarios, including mass wasting [68] and windstorms [14, 52–54, 70]. Three main phases and respective contributors have been identified during pullout tests of root systems: initial stiffness depending on material stiffness, surface area and projected area of the zone of rapid taper; ultimate capacity resulting from root cooperation emerging from synchronous mobilization of roots; and softening governed by the failure of individual roots and soil matrix during the propagation of loads throughout the root–soil system affected by root diameter and orientation [9]. As tension is transferred to the soil media through friction at the root–soil interface, an optimal morphology for resisting pullout is a root system with numerous fibrous roots, which enable a quick load transfer to the soil media through an increased surface area [27].

To ensure anchorage, the soil must also be maintained in place. Distributing structural loads more evenly throughout the granular media reduces the development of local stress concentrations and minimizes excess soil deformation and rearrangements. As a result, the soil at the edge of a dense packing of roots in a small volume may fail when pulled upward [8]. In a sloped environment or locations subjected to soil shearing, the root system consolidates the surface layers of the soil on which it is anchored by reaching deeper soil beyond the shear failure zone [13, 32, 61]. Root

systems impact on soil stability has been studied in different settings [12, 13, 32, 61]. While the presence of root systems is believed to reduce soil erosion and stabilize it [1, 4, 33, 35, 61, 74, 76], different root systems' geometries will have varying impacts. In order to understand the impact of their complex geometries on soil stability and anchorage, they must be broken down into specific characteristics, such as root diameter, total root length, root density and minimal bounding box encompassing the entire root system [7, 62]. The analysis of these characteristics can reveal trends enhancing anchorage and soil reinforcement. These trends could then lead to the use of specific tree species to increase soil stability in at-risk locations or the design of root-inspired structures. The principles of granular mechanics can serve to study the interactions between roots and soil particles. However, the complex morphology of root systems highly varies depending on species and environmental conditions, making the discovery of trends not straightforward [49]. In a direct comparison, root systems in their natural environment were shown to be 8 or 13 times more resistant to upward tension than micropiles and 43 or 70 more than shallow footings per volume or mass basis [9].

Since tree root morphology cannot be modified to analyze the effects of different root traits on anchorage or soil stability, simplified 3D models of branched rootlike structures with a taproot and laterals stiffer than their biological counterpart are often designed for numerical or physical tests [20, 21, 47, 49, 73]. In comparison with a simple vertical pile, the presence of laterals significantly increases anchorage [21, 48, 49]. A study found that the addition of laterals increased by more than three times the upward resistance [73]. The location of the laterals, especially their depth, heavily impacted test results [49]. To address the lack of research on the effect of material stiffness on pullout behavior, tests on rubber and wooden root analogs were conducted and showed that stiffer models (i.e., wooden) generated higher pullout resistance than the rubber ones and that shear strength was mobilized progressively in rubber models, but more rapidly and evenly throughout in wooden ones [49]. Therefore, stiff root analogs are expected to be more efficient at consolidating unstable slopes at small displacements, whereas more flexible ones seem more appropriate for large displacements. Similarly, another study found maximal reinforcement is reached before a displacement of 5 cm in fine roots but can happen after a displacement of 10 cm in a 20-mm-diameter root [64]. Despite the effect of materiality, branching increases slope reinforcement by resisting large loads during the beginning of slope failure [5, 69]. Root number and branching have been identified as important traits of biological roots to increase shearing resistance, while root cross-sectional area was not as efficient [32]. A finite element method study found that while characteristics leading to optimal pullout resistance differed based on the root pattern studied, laterals' number and diameter were the major contributors to pullout resistance overall [21]. In a shallow medium, root-inspired fractal anchors were found to be 2.6 times more efficient than a circular plate anchor, showing the effect of material distribution on mobilizing larger volumes of soil [24]. Overall, studies on root systems, root analogs and mathematical models of root–soil interactions have shown that pullout resistance is affected by characteristics at the root system scale (e.g., depth, branching, root dry mass, section of roots at the base and root number) and at the individual roots scale (e.g., root strength, soil strength, root–soil contact area, material stiffness, root diameter, tortuosity and surface roughness) [9, 19, 25, 26, 46, 47, 49, 50, 64, 65, 69, 76,]. With the goal of transferring valuable root data toward the design of foundation systems, each root trait should be analyzed separately in controlled experiments in order to understand their individual contributions to anchorage and soil reinforcement. Once basic principles are understood, the advantages of multiple traits can be combined to generate efficient morphological complexity to address specific design scenarios.

This work investigates the pullout resistance of branched root-inspired foundation systems. Abstract root-inspired pile morphologies were designed and 3D printed to evaluate the effects of five root traits of interest on pullout resistance: root length (i.e., length of laterals), number of branching locations (i.e., nodes), number of lateral roots at each branching location, branching angle (i.e., departure angle) and cross section of lateral roots. These traits were selected for their: expected contribution to anchorage and soil erosion prevention, ability to be tested in a controlled experiment and relevance toward foundations. Each model was designed starting from a main straight pile (i.e., taproot analog) from which different morphologies of branches (i.e., laterals) with various root traits emerge. Each root trait was analyzed from abstracted values (i.e., not values obtained from actual root systems). The goal was not to reproduce exact root morphology, but to achieve a clear understanding of the impact of each root trait and their variation on the pullout performance of the root-inspired pile foundation. Here, principles of granular physics, commonly utilized to analyze soil erosion and cohesion [59], served to analyze the interaction between the branched pile and the granular media. Vertical pullout resistance was evaluated by placing the 3D models inside a cylinder filled with dry sand and pulling them vertically. Force and displacement data were collected throughout each test, from which the following quantities are derived: maximum force resisted by the model, displacement at maximum force, work done throughout test, slope of the

force/displacement curve at 50% of maximum force (i.e., stiffness) and magnitude of the force/displacement curve's slope at 75% of maximum force after the peak (i.e., softening). These results were then compared to the root traits studied and the overall models' properties (i.e., embedded volume, embedded surface area and surface area of the model's vertical projection). The latter property refers to the surface area of the model's silhouette when viewed from the top (Z axis). The results would inform the type of data to extract and transfer from root systems as an initial step toward foundation designs with particular interest for structural support and erosion prevention. The knowledge gathered is especially relevant for anchors and similar structures subjected to upward loading.

2 Materials and methods

2.1 Pullout testing setup

Tests were performed with an overall setup similar to Mallett et al. [47] but with slightly larger chamber. The chamber used in this study is a clear acrylic cylinder with an internal diameter of 15 cm and a height of 30 cm. The chamber was filled with dry sand for a height of 25 cm. Each model was submerged with the bottom of the pile at an embedment depth of 18.25 cm and an extra 6.75 cm height of sand underneath to reduce the effect of the chamber floor. A graded standard Ottawa silica sand HM-108 (fine-grained sand), graded between No. 30 (600 μm) and No. 100 (150 μm) sieves, was used (Global Gibson, Inc., Nashville, TN, USA). Mean diameter (d_{50} = 494 μm) was calculated from 833 grains of sand measured with VHX 7000 digital microscope (Keyence Corporation of America, IL, USA). The sand particles' angle of internal friction (φ = 35°) was calculated with a standard direct shear test.

2.2 Root-inspired foundation pile models tested

Evaluating the effect of root traits on anchorage is not straightforward, since keeping one morphological variable constant across all models to produce comparable data will modify other variables. Previous studies testing the effect of branching angle and number of branches designed models of constant width and depth with lateral branches emerging at the bottom of the vertical pile by changing the length of the laterals and the pile [47, 73]. In a numerical study, simplified root patterns of varying morphologies scaled to possess the same volume led to significant variations in uprooting resistance of models with same morphology but different scales [21]. To facilitate comparison of test results between morphologies, each model was designed with the same base, such that the models' properties (i.e., volume, surface area and projection area in the direction of loading) serve to normalize the results during the data analysis. No property was kept constant between all models as it would introduce morphological variabilities between models, such as diameter of main pile and laterals, their depth or branching angle. Yet, multiple models still share similar model properties as they are built through the same parametric process (e.g., models "θ_{45}" and "θ_{135}" with respective branching angles of 45 and 135°). The direct effect of the root trait was therefore further analyzed for these models in one-to-one comparisons. Each model had the same main vertical pile with a diameter of 0.75 cm from which lateral branches emerge. Furthermore, one model "X_x" (highlighted in black in Fig. 1 and labeled as "$L_{4.5}$," "N_1," "B_3," "θ_{45}" or "S_o" depending on the trait studied) served as a control by being present in all five sets of root traits. The control model has 3 laterals with a circular cross section measuring 0.40 cm in diameter and 4.50 cm in length, pointing downward at an angle of 45° from the main pole orientation from a node located 12.25 cm deep (i.e., under the soil surface). A model "X_0" with no lateral branches served as a second reference for most root traits (highlighted in red in Fig. 1 and labeled as "L_0," "N_0," "B_0" or "θ_0" depending on the trait studied).

2.3 Root traits analyzed

Differences between each model are presented in Fig. 1. All models were parametrically generated in Rhinoceros (Robert McNeel & Associates, Seattle, WA, USA) with the Grasshopper plugin (by David Rutten at Robert McNeel & Associates) to only modify the geometry relating to a root trait analyzed. Each set (i.e., L, N, B, θ and S) focused on a different root trait, respectively: length of the laterals, number of nodes along main vertical pile, number of laterals at one node, branching angle and cross section of laterals. For the laterals' length, model "L_0" has no laterals, while the other models possess laterals of either 2.25 cm for "$L_{2.25}$," 4.50 cm for "$L_{4.5}$" and 6.75 cm for "$L_{6.75}$." The second set tested the difference between having 3 laterals emerging from zero node (i.e., no laterals in "N_0"), one node in "N_1" or two nodes in "N_{2a}" and "N_{2r}." The difference between models with two nodes is that the laterals in "N_{2a}" are aligned on top of each other, while in "N_{2r}" they are rotated 60° horizontally to not be overlapped. The distance between both nodes is 6 cm, which equals around 121 sand particles on top of each other. Upper and lower nodes are located 6.25 and 12.25 cm under the soil surface. For set B, the number of laterals (i.e., branches) was zero in "B_0," one in "B_1," three in "B_3" and six in "B_6." These laterals were

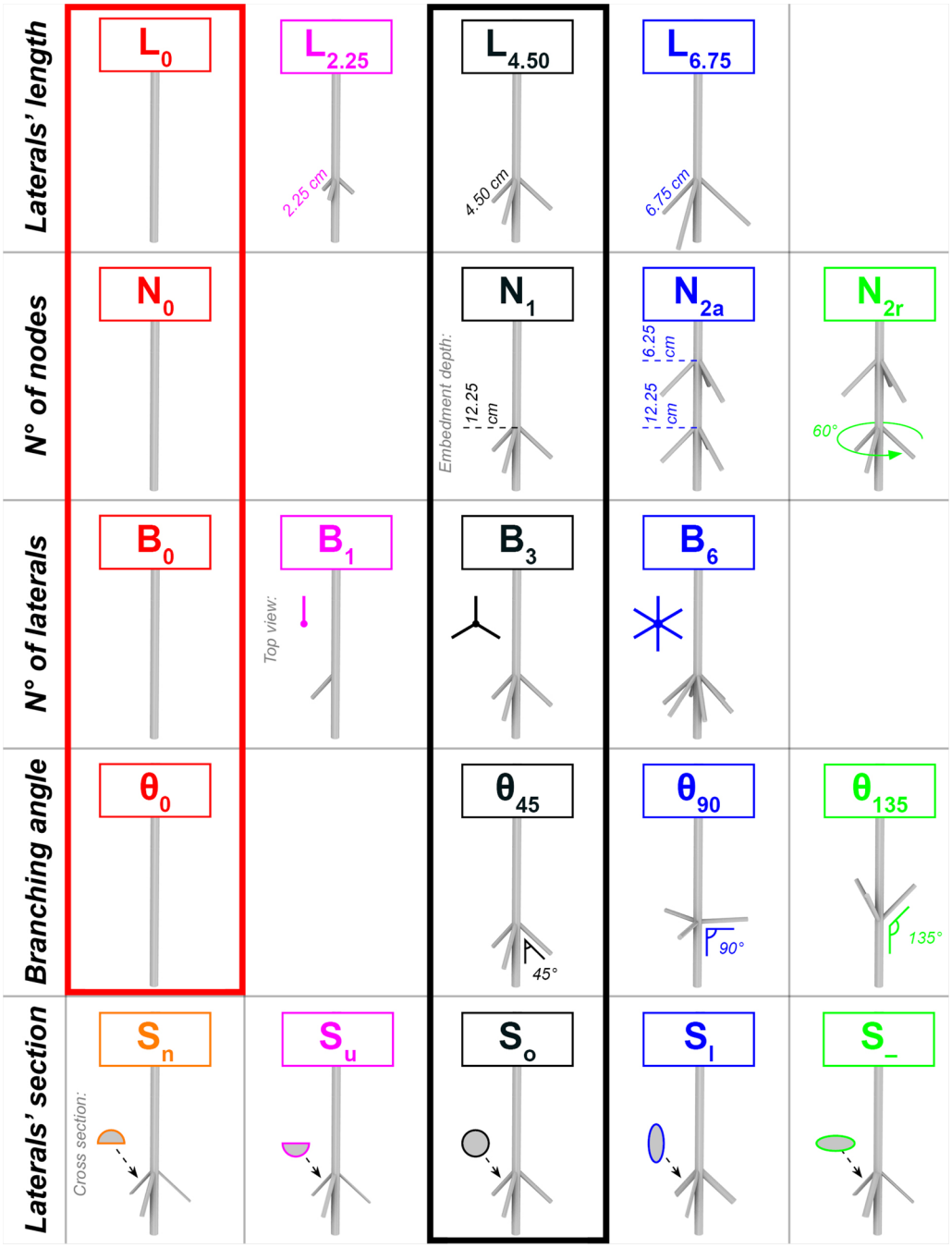

Fig. 1 Models tested in five sets studying the following root traits: laterals' length (L), number of nodes (N), number of laterals (B), branching angle (θ) and laterals' cross section (S). One model (also named "X_x" highlighted in black) is common to all sets and serves as a control. Another reference model "X_0" is present in four sets (highlighted in red) (color figure online)

equidistantly distributed around the main pile with 120 or 60° between laterals for models with three and six laterals. In comparison with the orientation of the main vertical pile, branching angles ranged from 0° in "θ_0," 45° in "θ_{45}" (i.e., downward), to 90° in "θ_{90}" (i.e., horizontal) and 135° in "θ_{135}" (i.e., upward). Differences between five cross sections of laterals were evaluated: upper semicircle in "S_n" (i.e., flat part facing down), lower semicircle in "S_u," circle in "S_o," vertical ellipse in "S_l" (i.e., main axis oriented vertically) and horizontal ellipse in "S_." The cross-sectional areas of the circle and ellipses were equal. For the ellipses, the longer radius was 2.25 times larger than the smaller one. The semicircle cross sections were obtained by removing the upper or lower half of the circle, which means that their cross-sectional areas equaled half of the circle and ellipses' areas.

2.4 Manufacturing the models

The models were 3D printed with stereolithography to produce a smooth surface and reduce frictional resistance between sand and model. The models were printed with the gray resin V4 on Form 2 and Form 3 printers (Formlabs, Somerville, MA, USA). Models were then soaked in Isopropyl Alcohol for 1 h to clean impurities at the model's surface. They were then cured for 30 min at 60 °C in the Form cure, arriving a modulus of elasticity of around 2.2 GPa (Formlabs, Somerville, MA, USA). Supports were only removed after this step to maintain model morphology during the post-printing process. Imperfections left from supports and printing process were sanded to compare models with similar surface roughness.

2.5 Size ratios between the setup and models' dimensions

Modifying the boundaries of the chamber containing the granular particles will influence the spatial distribution of the force chains, as seen with the Jansen effect [66]. The ratios between the radii of the chamber, models and particles are therefore important to minimize the effect of the boundaries on the test results. Previous physical and numerical studies have used a wide variety of: chamber-to-model ratios ranging from 2.28 [47] and 11 [30] for branched models, up to 18.05 [39] and 52 [17, 31] for unbranched ones; and pile-to-particle radius ratios ranging from 3.04 [39] and 10 [30] up to 51.2 [17, 31]. To evaluate the boundary effect and visualize strain fields in the soil media, researchers have used X-ray equipment or digital cameras to perform digital image correlation or particle image velocimetry analysis [17, 31, 44, 49] or discrete and finite element methods [20–22, 29, 40]. Combined computed tomography and digital image correlation analysis of pullout with branched models of chamber ratios of 2.28 have shown the effect of models' morphology on localized soil deformation fields which can extend to the boundary walls [47]. In their study, the shear strain volume and failure surface of a model with laterals angled at 45° could have been influenced by proximity with boundary walls, but the failure surface of models with laterals at 30° did not converge toward the boundary. In our case, the radii of models, calculated from their projection in the Z direction, varied based on their morphology from 0.38 to 5.00 cm. Therefore, the chamber-to-model radius ranged from 19.27 for the model with no laterals "X_0" (i.e., second reference model highlighted in red in Fig. 1) to 1.50 for the model with longer laterals (i.e., "$L_{6.75}$"). Since this study evaluates the effect of different root traits (e.g., laterals' length, number of laterals and branching angle), the width of some models varied from the reference ones. Keeping a constant width for all models would have needed to be compensated by increasing morphological variability between models. The main vertical pile-to-particle radius ratio in our setup equals 15.18 and chamber-to-particle radius ratio 303.64. Based on these ratios, boundary effects are likely present, but not expected to be the dominant factor distinguishing the performance of the different models. The edge of the largest model (i.e., "$L_{6.75}$") was at a distance of 50 particles from the boundary. During the tests, no particle rearrangement was observed along the boundary from digital images taken through the transparent boundary.

2.6 Pullout testing procedure

The model, clamped to the load cell, was lowered inside the empty chamber. Each model was then locked in place at the top of the chamber to restrain its movement while filling (Fig. 2a). For each test, the sand was placed in the chamber through the same procedure to achieve equivalent packing fractions. One-fourth of the chamber was filled with sand, and the sides of the chamber were then tapped with a rubber mallet a total of 40 times (i.e., 10 on each side: right, left, back and front) at two different heights: around 5 cm above the bottom of the chamber and around 5 cm under the soil surface. The same tapping procedure was repeated after filling each quarter of the chamber with sand. When all the sand was in place (Fig. 2b), a brush was used to even the soil surface, followed by another set of 40 taps 5 cm under the soil surface. The calculated void ratio was 0.70 with a relative density Dr (%) of 53%, corresponding to a medium-density sand. The pullout tests were performed with a 5582 Instron with a 500N 2525-816 Instron load cell (Instron, Norwood, MA, USA). Each model was tested three times, and the mass of sand was measured at the beginning and end of each test day. The highest loss of sand observed during one day of test was 3.1 g out of the 6,870 g used for testing. The mass of sand lost was added before the next day of testing. Tests were performed at room temperature with a temperature ranging from 23.9 to 27.5 °C and relative humidity from 30 to 37%. Each model pulled out of the sand vertically at a constant speed of 1 cm/min, to match a similar study and produce comparable results [47]. At a rate slower than 10 cm/min, the granular media is not considered to be fluidized [37]. Therefore, the drag force observed during the pulling out test is mostly dependent on frictional and normal forces between particles and obstruction (i.e., model), and between particles (i.e., depending on their surface roughness, morphology, gravity, mass of the grains) [3]. Once the model was fully out of the sand, the force measurement slightly varied between tests due to variations in the filling process and resulting force applied

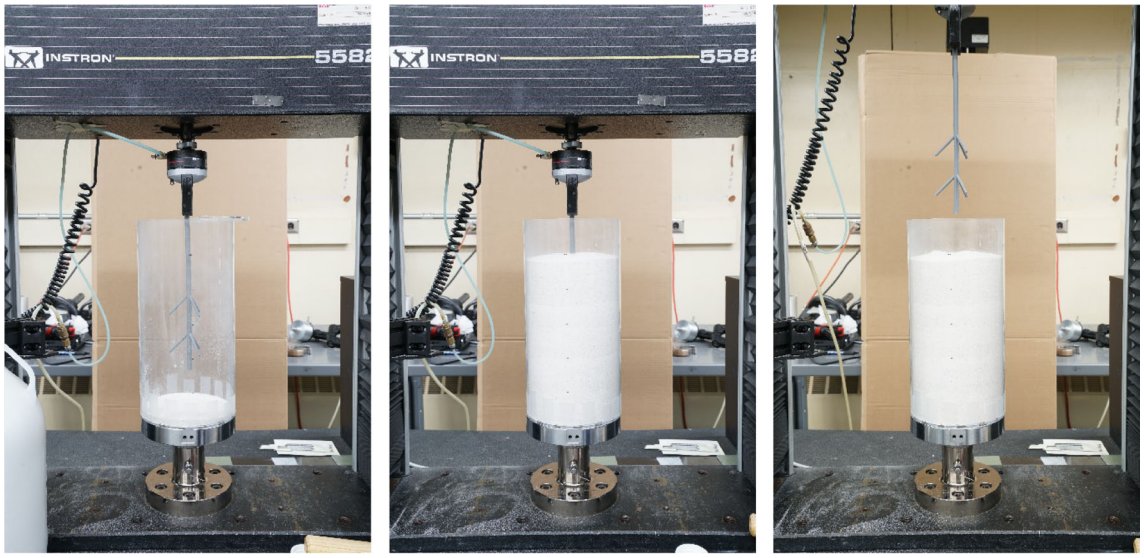

(a) (b) (c)

Fig. 2 Setup used and the main steps of the pullout test procedure. Model "N_{2a}" is lowered inside the empty chamber and locked in place (**a**). The chamber is filled with sand with a specific filling and tapping procedure (**b**). The model is slowly pulled upward at a rate of 1 cm/min until it comes out of the sand (**c**)

to the submerged model (Fig. 2c). Therefore, the force data of each entire test were shifted, so that it would equal 0 at the end of the test. This shift made the data comparable and removed the weight difference of the various models to only measure the force acting on each model. The data analysis was then performed on this tared force data.

2.7 Data analysis

Force–displacement curves of models pulled out of dry sand are jagged due to localized avalanches of the granular media or stick–slip mechanism [49]. For each model, the three force–displacement data, corresponding to the three tests performed, were averaged. The averaged force–displacement data were then smoothed in python to generate a force–displacement curve from which test results could be extracted. Diverse smoothing methods were assessed, and a spline method was selected due to its higher fidelity to the original data. In addition, the three force–displacement curves representing the three tests for each model were individually smoothed using the same method to extract: Fmax (N) (i.e., maximum force reached), displacement at Fmax (mm), work (J) (i.e., area under the force/displacement curve), tangent stiffness (i.e., slope of the force–displacement curve at 50% of Fmax) and softening (i.e., magnitude of the force–displacement curve's slope at 75% of Fmax after the peak). These properties, selected due to their direct relevance for foundations systems, were then averaged per model for cross-model analysis to draw mechanistic understanding of the phenomena. Based on the models' material properties, the deflection of the laterals' tip was also calculated for the maximum force resisted by each model. Laterals were considered as angled cantilever beams with a uniform dead load acting upon them. First, the contribution of the main pile to pullout resistance through frictional resistance (i.e., gathered by testing the unbranched reference model "X_0") was subtracted to extract the force applied to the laterals. The maximum force was then divided by the number of laterals present on each model and converted into an angled uniform dead load along the length of each lateral. Finally, the deflection at the tip of the laterals of each model was calculated from this angled uniform dead load, the lateral's moment of inertia, the lateral's length and the modulus of elasticity of the material. The results were compared to the overall model properties, and further separate analyses were performed to study the effect of each root trait.

3 Results and discussion

3.1 Overall results across all sets

The averaged and smoothed force–displacement curves for all models across the different sets are presented in Fig. 3. Overall, peak force was reached within 8 mm of vertical displacement. Mobilization of the entire system to resist peak loading depends on material and soil stiffness, geometry and loading direction, and was observed within 7 cm of vertical displacement of root systems tested in

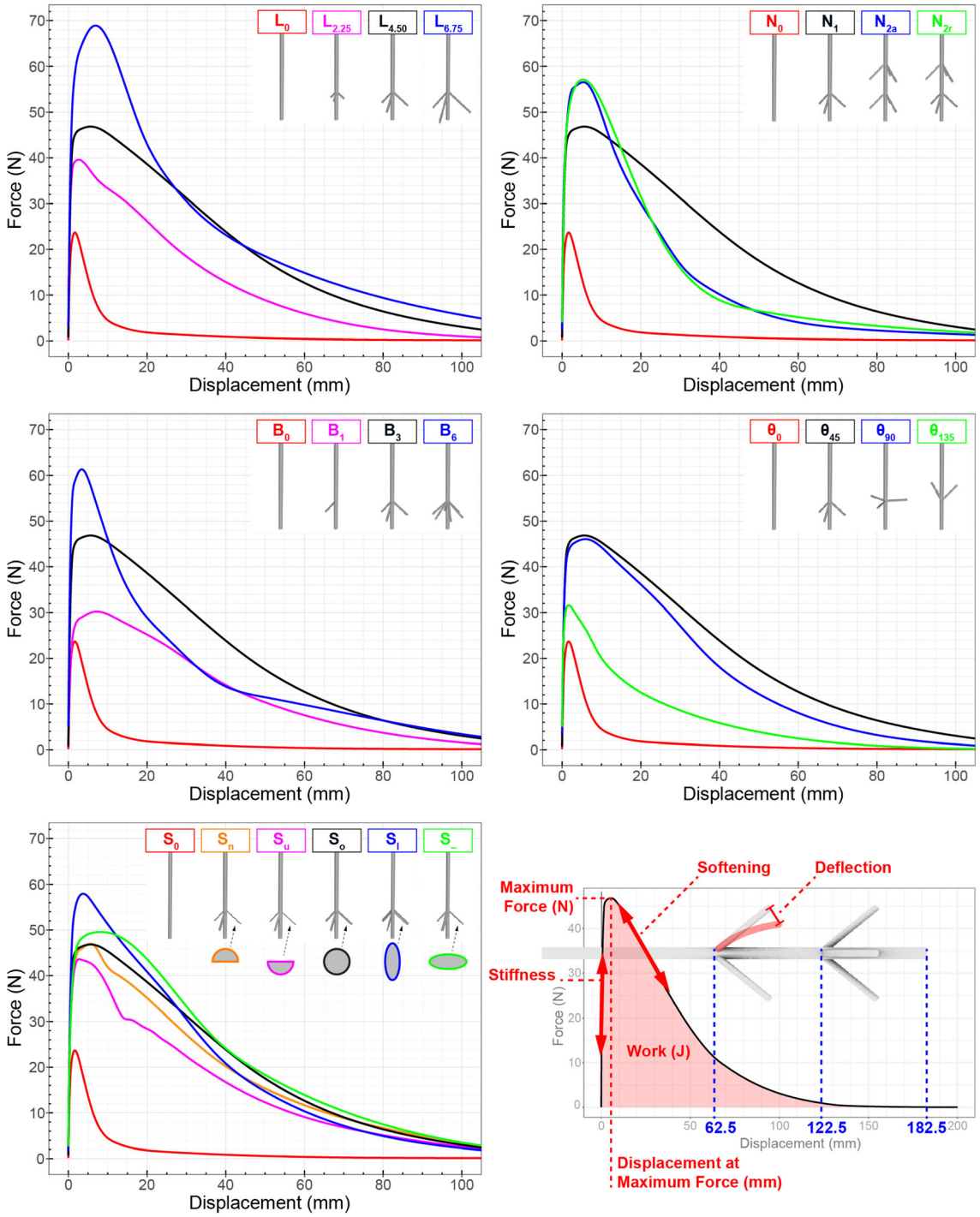

Fig. 3 Force–displacement curves for each set (i.e., root trait) analyzed: laterals' length (top left), number of nodes (top right), number of laterals at one node (middle left), branching angle (middle right) and laterals' cross section (bottom left). Each curve represents the smoothed average of the three tests conducted for this specific model. The curves of both reference models are shown in black for "X_x" and red for "X_0" for each trait. The bottom right panel displays the force–displacement curve for reference model "X_x" from which maximum force, displacement at maximum force, work, stiffness, softening and deflection are extracted (red). A side view of model "N_{2r}" is shown as a reference to visualize at what displacement each node comes out of the sand surface (blue) (color figure online)

their natural environment [9]. The force resisted dropped drastically after reaching peak force, characterized by the reduction in root–soil friction, contact area and shear strength as the model started to move [21, 49, 64]. In comparison, root systems pulled out of their natural soil sustained most of the peak tensile force even past 25 cm of

Table 1 Properties and test results of each model. Both reference models common to the different sets (highlighted in red and black) are shown in the top rows. Reference model "X_0" is also known as "L_0," "N_0," "B_0" or "θ_0" and "X_x" as "$L_{4.5}$," "N_1," "B_3," "θ_{45}" or "S_o" from Fig. 1, depending on the trait studied

Model	Model properties			Test results					
	Volume (cm^3)	Surface area (cm^2)	Z projection surface area (cm^2)	Maximum force (Fmax) (N)	Displacement at Fmax (mm)	Calculated deflection of laterals' tip at Fmax (mm)	Work (J)	Stiffness	Softening
X_0	**8.08**	**43.56**	**0.44**	**23.84 ± 1.09**	**1.66 ± 0.17**	**N/A**	**215.48 ± 27.52**	**31.92 ± 0.85**	**3.80 ± 0.69**
X_x	**9.59**	**58.50**	**3.97**	**46.82 ± 1.04**	**5.68 ± 0.68**	**1.21**	**2171.40 ± 57.59**	**56.17 ± 4.64**	**0.69 ± 0.11**
$L_{2.25}$	8.74	50.02	2.06	39.78 ± 2.01	2.18 ± 0.49	0.07	1340.58 ± 65.99	52.98 ± 5.86	0.79 ± 0.14
$L_{6.75}$	11.28	75.46	7.78	68.80 ± 0.93	7.16 ± 0.29	8.90	2684.94 ± 25.00	46.24 ± 2.23	2.47 ± 0.24
N_{2a}	11.09	73.44	3.97	56.68 ± 1.60	5.24 ± 0.38	0.86	1526.86 ± 7.35	49.72 ± 5.93	2.29 ± 0.41
N_{2r}	11.09	73.44	7.49	57.23 ± 0.43	5.81 ± 0.13	0.88	1598.32 ± 10.79	43.27 ± 2.17	1.94 ± 0.10
B_1	8.59	48.54	1.62	30.19 ± 2.38	6.84 ± 0.13	1.00	1339.98 ± 106.98	26.24 ± 2.14	0.54 ± 0.02
B_6	11.09	73.41	7.49	61.34 ± 0.48	3.24 ± 0.10	0.99	1867.88 ± 25.72	65.87 ± 7.26	2.81 ± 0.47
θ_{90}	9.64	59.20	5.41	45.99 ± 3.82	5.73 ± 1.04	2.44	1789.80 ± 115.10	49.36 ± 5.04	0.96 ± 0.20
θ_{135}	9.59	58.50	3.97	31.44 ± 1.47	1.68 ± 0.24	0.40	722.49 ± 21.03	57.10 ± 4.05	1.48 ± 0.20
S_n	8.85	56.06	3.97	47.00 ± 1.52	5.64 ± 0.11	2.44	2006.38 ± 35.92	37.74 ± 3.72	0.77 ± 0.09
S_u	8.82	55.59	3.83	43.51 ± 2.64	3.00 ± 0.22	2.07	1675.55 ± 73.23	49.29 ± 4.08	1.60 ± 0.17
$S_\|$	9.58	60.30	2.83	57.98 ± 2.03	3.71 ± 0.13	0.79	2153.92 ± 82.13	53.05 ± 0.89	1.06 ± 0.12
$S_\_$	9.60	60.50	5.71	49.69 ± 0.53	7.73 ± 0.54	2.95	2344.48 ± 61.46	37.67 ± 3.51	1.13 ± 0.10

upward displacement [9]. Simplified 3D models of root-inspired piles lack higher order roots and have a larger ratio between laterals and sand particles, compared to the ratio between biological roots (i.e., including fine roots) and soil media [10]. Furthermore, the absence of cohesion in the sand particles likely led to fluidization after peak force. Major variations can be observed between the pullout resistance of the different models analyzed. By observing these curves, the variations in laterals' cross section had the lowest effect on pullout resistance. To study the detailed effects of each root trait on pullout resistance, the different types of measurement extracted from these curves are shown in Fig. 3 and analyzed in the following sections.

Table 1 shows the test results of each model along with their properties. Each model was tested 3 times (n = 3). Overall, some correlations were observed between most models' properties and test results (Fig. 4). Maximum force increased with increasing embedded volume (RSquare = 0.75), surface area (RSquare = 0.82) and Z projection area (RSquare = 0.68). Out of these three models' properties, surface area had the strongest correlation while Z projection area had the weakest. A greater surface area in contact with soil particles increases the amount of soil to be mobilized by shear through skin friction [9]. Regression analysis showed the lack of correlation between the models' properties and the other test results, with RSquares less than 0.41. No trend was observed between the displacement at maximum force and the models' properties. As a combination of both former parameters (i.e., Fmax and displacement at Fmax), stiffness generally increased with larger models' properties. Softening was high for the model without branches. The models with branches followed an upward trend: as models' properties increased, softening generally increased, but remained lower than that of the unbranched one. Higher volume, surface area and Z projection area generally led to increased work when considering all models. The projection area in the Z direction was expected to be a better indicator of maximum pullout resistance than embedded volume and surface area of the pile, as it represents the

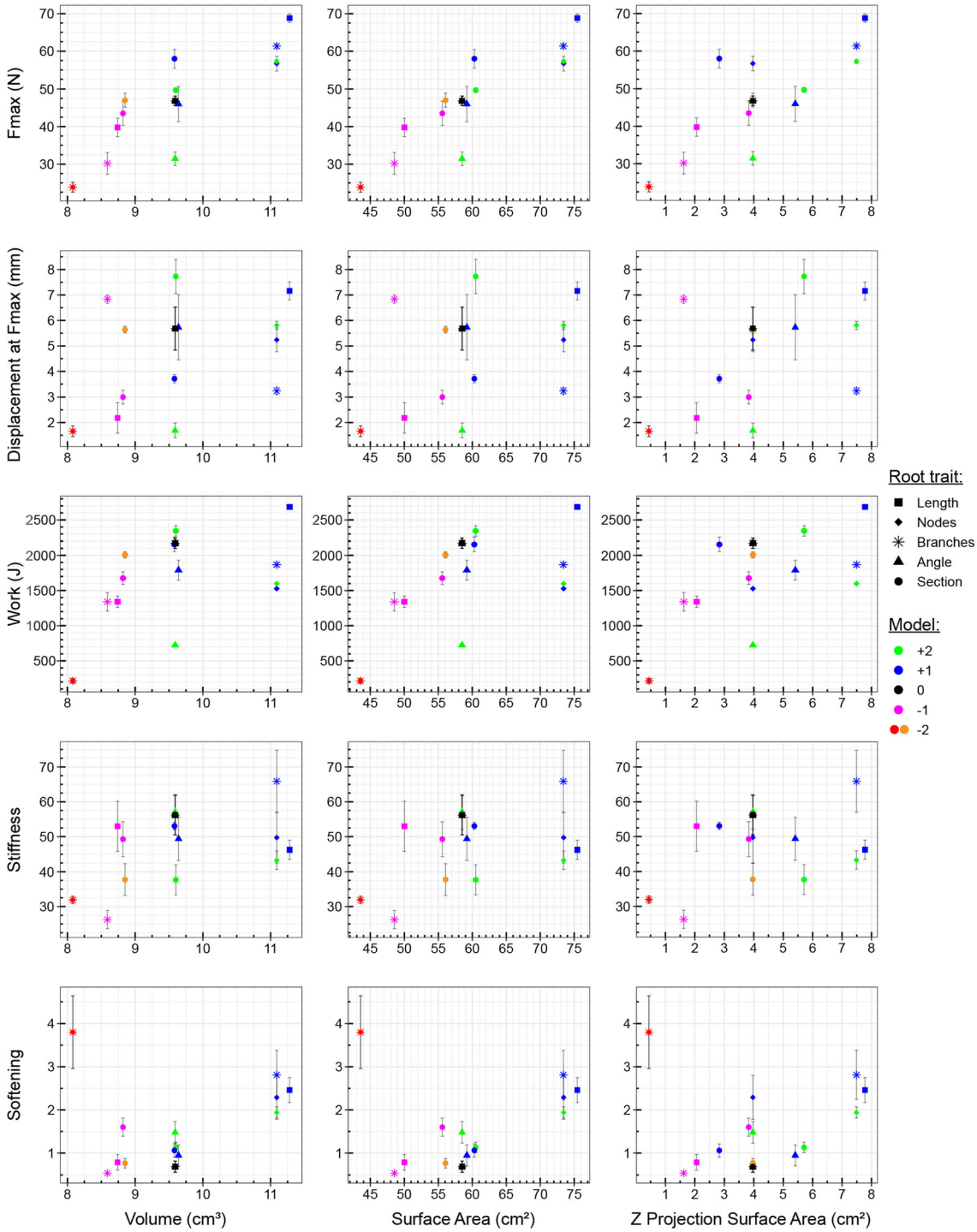

Fig. 4 Effects of embedded volume (left), embedded surface area (middle) and Z projection area (right) on the maximum force, displacement at maximum force, work, stiffness and softening. Different symbols represent the various sets (i.e., root traits). Colors refer to the different models for each trait, as seen in the columns of Fig. 1, going from the left column (" − 2"), to the middle left one (" − 1"), to the center one for the control model ("0"), to the middle right one (" + 1") and finally the right column (" + 2")

model's bearing area. Yet, out of the different model properties analyzed, Z projection area was not a better indicator of pullout resistance than volume and surface area (Fig. 4). All models tested except one are branched with lateral(s), meaning that they already take advantage of an increased Z projection area to increase bearing capacity. When directly comparing branched to unbranched models, the Z projection area serves as better indicator than volume

and surface area. For instance, increasing the volume of a straight vertical pile will increase the frictional surface area between the model and the sand particles, but its resistance will only still rely on frictional forces. However, adding laterals increases bearing area and resulting resistance via normal forces. While overall trends were observed, they did not apply to all models and specific relationships with varying root traits were not trivial. Since the test results cannot only be explained by the overall model properties analyzed, the effects of each root trait on pullout resistance were evaluated in separate analyses. In the following sections, the observed results for each root trait are reported along with qualitative interpretations based on basic principles of granular physics.

3.2 Effects of laterals' length on pullout resistance

Out of all the traits studied, the effect of laterals' length was the most straightforward. As expected, the length of laterals was positively correlated with Fmax, displacement at Fmax and work for the values tested in this work (Fig. 5). Due to the downward orientation of the laterals, the number of particles between the soil surface and the laterals' tip is greater than between the soil surface and the laterals' base. As a result, longer laterals angled downward possess an even larger volume of soil on top of them compared to if they were horizontal (i.e., perpendicular to the loading direction). The larger estimated deflection at the tip of longer laterals could be a reason for the increased displacement required to reach Fmax. 6.75-cm-long laterals (i.e., model "$L_{6.75}$") lead to slightly higher Fmax compared with the trend observed with 2.25 and 4.50 cm laterals, while displacement at Fmax was slightly lower than that trend. Stiffness was highest for the model with laterals measuring 4.50 and 2.25 cm in length. The opposite trend was observed for softening with lowest values for model "$L_{2.25}$" and "$L_{4.5}$." Model "$L_{6.75}$" model showed a reduction in stiffness and an increase in softening. Longer laterals are located closer to the chamber wall. The corresponding larger deformation field around the model could interact with the chamber walls based on the Janssen effect [66].

3.3 Effects of number of nodes along the main pile on pullout resistance

An increase in the number of nodes along the main pile was expected to increase overall pullout resistance. The addition of nodes significantly increased the maximum force (Fig. 6). Going from zero node to one node significantly increased displacement at Fmax, work and stiffness but decreased softening. However, adding a second node slightly lowered displacement at Fmax and significantly decreased work and stiffness but increased softening, in comparison with the model with one node.

A model with no node (i.e., no laterals) only resists pullout through frictional forces against the surface of the main pile. For models with nodes, the displacement at Fmax was similar for one or two nodes. This displacement depends in part on the size of the deformation field before the soil yields around the motion of the model. Deflection

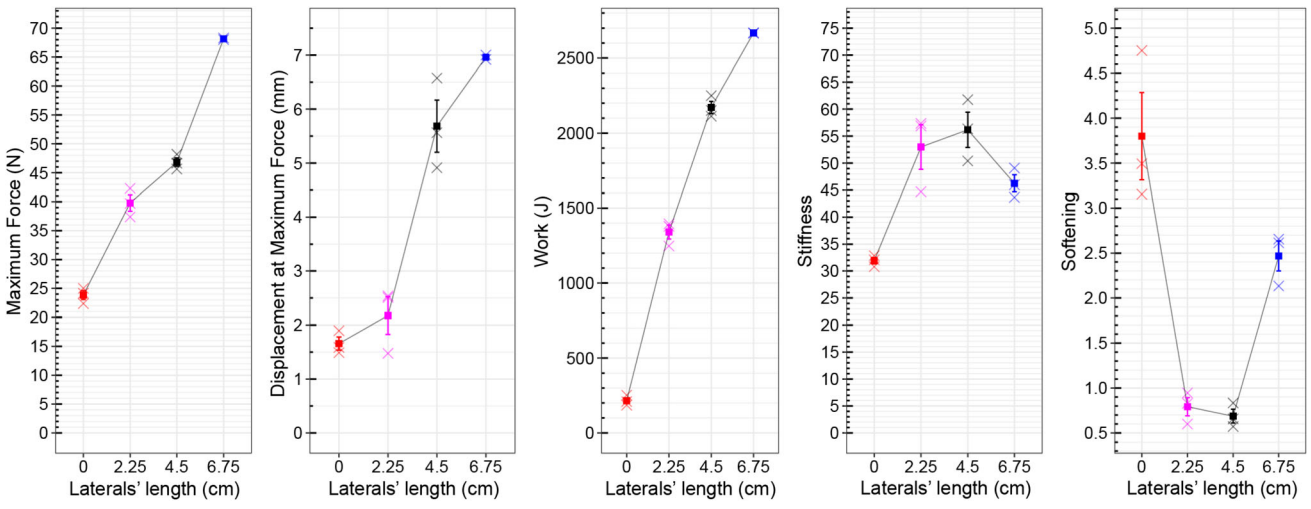

Fig. 5 Effects of laterals' length on the maximum force, displacement at maximum force, work, stiffness and softening. The four lengths tested were 0 cm (meaning no laterals, "L_0" in red), 2.25 cm ("$L_{2.25}$" in purple), 4.50 cm ("$L_{4.5}$" in black) and 6.75 cm ("$L_{6.75}$" in blue). Means and standard deviations are presented with three replicates (X data points) for each model (color figure online)

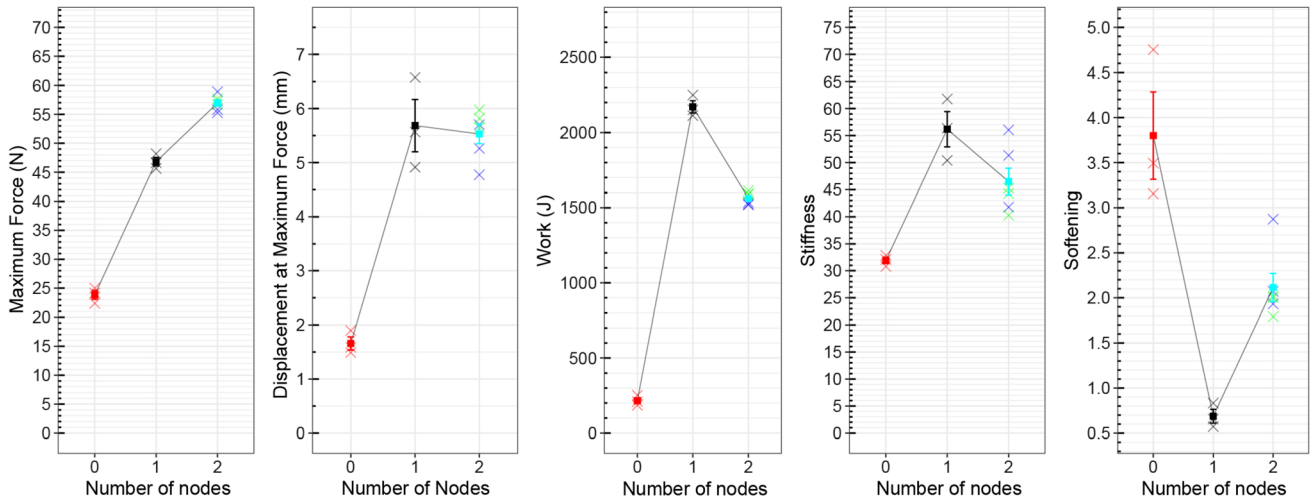

Fig. 6 Effects of number of nodes on the maximum force, displacement at maximum force, work, stiffness and softening. Models possessed zero ("N_0" in red), one ("N_1" in black) or two nodes (in turquoise, with data points for "N_{2a}" in blue and "N_{2r}" in green) (color figure online)

at the laterals' tip could also affect the displacement at Fmax. This deflection was estimated to be relatively low for these models, ranging from 0.86 mm for "N_{2a}" and 0.88 mm for "N_{2r}" to 1.21 mm for "N_1." Models with two nodes resisted higher maximum force, but took less work to pull out, displayed lower stiffness and greater softening compared to those with only one. This observation may be understood by considering the laterals' role in the jamming transition [6]. With only one lower node, the model pushes against largely jammed soil for a longer period of the test. However, when two nodes are present, the upper node breaks through the soil matrix, disrupting the network of force chains developed in the soil's initial preparation. Once the lower node reaches this part of the loosened sand, the force required to move through this unjammed soil is lower, leading to lower work overall. Furthermore, a greater depth of the root system greatly increases pullout resistance due to the added weight of sand above it [49, 69]. Due to the depth difference (i.e., closeness to the surface), the upper node acts against a smaller volume of soil than the lower (i.e., deeper) node. This decrease in volume along with the closeness to the soil surface would lead to a lower force required to break through the upper part of the granular media.

Two models with two nodes were tested: "N_{2a}" with laterals on top of each other and "N_{2r}" with laterals rotated by 60°. While having the same volume and surface area, both models have a different Z projection area. Along with the Z projection area, the volume of soil above the immersed laterals (i.e., volume directly in the projected path of the model being pulled upward) is also smaller when the laterals are aligned (45.49 cm^3 for "N_{2a}") compared to when rotated (73.42 cm^3 "N_{2r}"). As a result, "N_{2a}" was expected to generate a decreased pullout resistance in comparison with "N_{2r}." However, pullout resistance was not significantly different between both models (Table 1). Therefore, the higher Z projection area did not increase pullout resistance in this case. Our observations are consistent with the notion that each lateral rearranges the granular structure in an influence zone smaller than the distance between the two nodes. In this study, the distance between both nodes equaled 121 sand particle diameters. In natural root systems, the cohesion of soils between laterals forms a solid root/soil plate [12]. This cohesion either generated by the cohesive nature of fine geomaterials or by the interaction of capillary forces, water content and interparticle friction in granular media. In this study, by contrast, the non-cohesive dry sand particles more readily flow around and between root elements. When both nodes are stacked in "N_{2a}," the laterals of the lower node pass through the granular media at the same location as those from the upper node. Due to the lack of performance difference between both models, sand particles could be resettling before the second node and its influence zone travels through them. However, they do not settle back to their original packing fraction (i.e., right after tapping the side of the chamber), as suggested by the comparison of models with one or two nodes. Another plausible reason is that the nature of the long-range interaction between the nodes is not significantly affected by the rotated angle. Visualization of the strain field would be necessary to validate the potential reason behind the results observed. Based on the results of this set of models, it can be assumed that the exact stacking of laterals does not affect the pullout resistance in this setting (i.e., scale, distance between nodes and material properties), but the presence of multiple laterals located at different heights

(i.e., multiple nodes along the main pile) will increase Fmax and softening while lowering work and stiffness.

3.4 Effects of number of laterals at one node on pullout resistance

An increase in numbers of laterals was expected to increase pullout resistance, as it enlarges the volume of mobilized soil particles [47, 73]. For the number of laterals at each node, Fmax was linearly correlated with the number of laterals for the values studied (i.e., 0, 1, 3 and 6), which relates to an increase in models' properties including bearing area (Fig. 7). Having laterals significantly increased the displacement at Fmax and work. However, the number of laterals from one to six decreased displacement at Fmax. Work significantly increased from one to three laterals but decreased from three to six. Softening followed an opposite trend compared to work. Stiffness decreased when one lateral was added to the main vertical pile. Yet, stiffness increased as more laterals were added. Therefore, the addition of laterals, and resulting increased bearing area localized around the node present, did not increase pullout performance for all result variables.

To understand the disparate results, two phases of the pullout test should be differentiated. Until maximum force is reached, the granular media remains jammed, and the deformation is distributed more evenly across the soil. An increase in bearing area localized at a specific depth (i.e., around the node) creates a larger obstruction around which the soil media must deform. Furthermore, soil arching between laterals is likely happening, as was suggested in a study observing volumetric shear strain with computed tomography technology. Crossing the maximum force, granular media unjams, and the deformation localizes, as soil particles flow around the model. For the model with six laterals, the force carried drops abruptly after reaching the peak, meaning that the additive effect of number of laterals dissipates. Therefore, adding laterals makes it harder for the model to start moving. Yet, once the system is in motion, the larger number of laterals appears to facilitate unjamming the particles and making it easier for the sand to flow. Furthermore, it can be observed that increasing the number of laterals from one to three and six decreases the displacement needed to reach peak force, demonstrating that increasing bearing area in this way can counterintuitively lead to smaller tolerance in displacement to unjamming the medium. Conversely, due to the absence of bearing capacity in a model with no laterals, only frictional forces can resist the movement, leading to a relatively low displacement needed to reach a relatively low Fmax. As soon as the model moves independently from the soil particles, parts of the frictional area are lost as a boundary effect is formed.

3.5 Effects of branching angle on pullout resistance

For the effect of branching angle (i.e., departure angle), laterals perpendicular to the main vertical pile were expected to increase pullout resistance in comparison with those angled diagonally, due to a higher Z projection bearing area [69]. An increase in branching angle from 30° to 45° resulted in an increase in the pullout capacity in another study, which could be due to the increased depth of the 45° laterals [47]. Yet, differences between angling laterals at 45° and 90° were not significant for Fmax and displacement at Fmax (Fig. 8). Between both models, laterals angled at 45° increased work and resulted in slightly

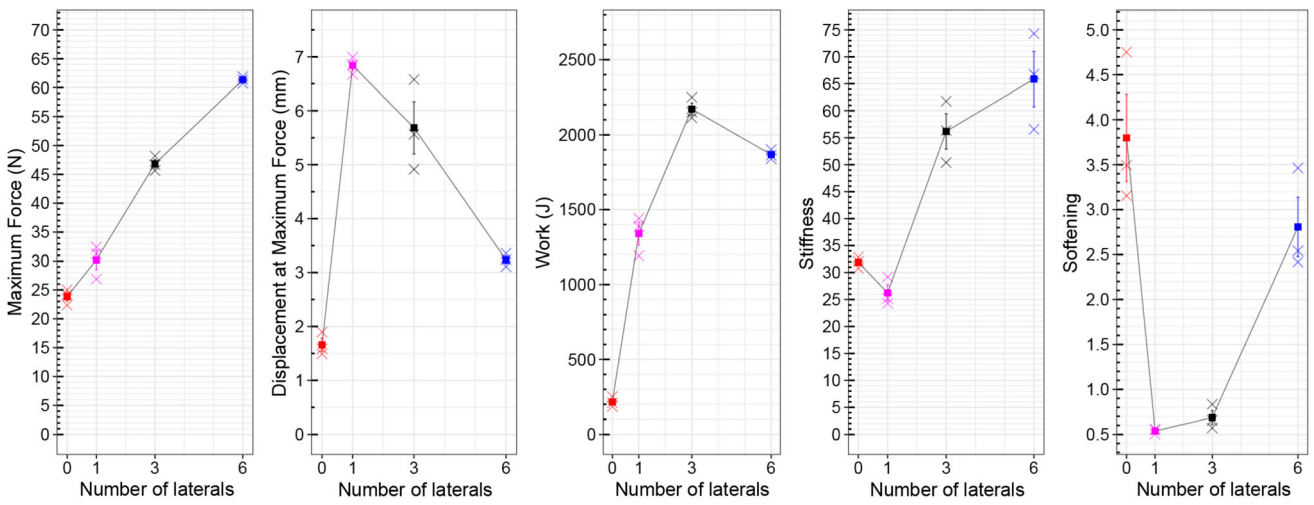

Fig. 7 Effects of number of laterals at one node on the maximum force, displacement at maximum force, work, stiffness and softening. Models possessed zero ("B_0" in red), one ("B_1" in purple), three ("B_3" in black) or six laterals ("B_6" in blue) (color figure online)

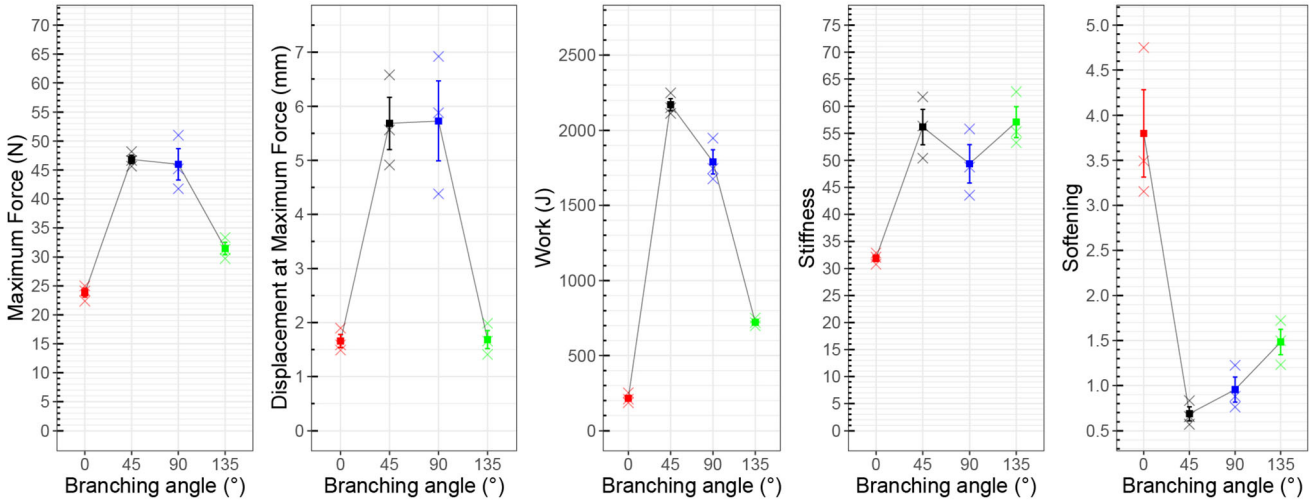

Fig. 8 Effects of branching angle on the maximum force, displacement at maximum force, work, stiffness and softening. Laterals were either angled at 0° (i.e., no laterals ("θ_0" in red)), pointing downward from the vertical pile at 45° ("θ_{45}" in black), perpendicular to it at 90° ("θ_{90}" in blue) or pointing upward at 135° ("θ_{135}" in green) (color figure online)

higher stiffness and lower softening. Out of the branched models, pointing the laterals upwards (i.e., "θ_{135}") led to a significant decrease in Fmax, displacement at Fmax and work, but showed a slight increase in stiffness (only compared to model "θ_{90}") and softening. Since the stiffness is calculated as the tangent's slope of the force–displacement curve at 20% of Fmax, the low maximum force resisted (Fmax) by model "θ_{135}" shifts the tangent stiffness measurement to an earlier part of the test (i.e., lower displacement), which could be a reason for an increased stiffness in this case.

Models "θ_{45}" and "θ_{135}" with laterals angled at 45 and 135° led to significantly different results, despite possessing the same following properties: volume, surface area and Z projection area. Despite sharing these same properties, a diversity of reasons can be used to interpret such results. As seen in models with laterals pointed downward, deflection of laterals under Fmax reduces the Z projection area. Inversely, the deflection of laterals pointing upward in "θ_{135}" would result in a slight increase in the Z projection area. However, the overall pullout resistance of model "θ_{135}" was lower than model "θ_{45}." The branching angle also affects the depth of the laterals' center of mass, the resulting volume of grain directly above them, the proximity to the soil surface and connection angle with the main pile in the direction of loading. Laterals angled upward have less volume of soil directly above them (i.e., in the path of pullout) than those pointing downward (37.18 cm^3 for model "θ_{135}" and 47.02 cm^3 for model "θ_{45}"). Therefore, the angle of the laterals is likely impacting the pullout resistance by changing the volume of impacted grain. Despite increasing the volume of soil above the laterals (61.45 cm^3 for "θ_{90}"), angling the laterals perpendicular to the main axis resulted in lower work compared to model "θ_{45}." Furthermore, the tips of laterals pointing upward can be thought to introduce highly focused stresses to disrupt force chains and loosen grains. This behavior could be seen as forming an analogous equivalent to micro fractures which would locally propagate throughout a solid continuum. In the reference model "θ_{45}," laterals are pointed downward meaning that their tips do not impose any opening the granular media in very localized regions. Another reason behind such results could be the difference in the depth of the laterals' center of mass since the node depth remains the same. This design parameter means that laterals pointing upwards extend toward the soil surface and support a smaller soil volume. In comparison with models "θ_{45}" and "θ_{135}," model "θ_{90}" has a slightly higher Z projection area due to the laterals being perpendicular to the main pile. Branching angles of 45° and 90° lead to similar Fmax and displacement at Fmax, but the laterals at a 90° angle result in a lower work. The former shows the resistance to pullout prior to soil rearrangement, which seems to be mostly driven by the size of the bearing area. In this case, the latter could result from the angle of the bearing area. After peak force, sand particles located along the bearing area of laterals perpendicular to the pullout direction fall under the model and will not serve the bearing capacity anymore. However, when laterals are angled at 45°, particles could slide along the sloped bearing area and contribute to the pullout resistance for the extent of pullout. This difference would lead to higher work. Another aspect to consider is the impact of the orientation of laterals on the influence zone. For instance, when the laterals are horizontal in model "θ_{90}," force chains are likely to extend upward. Angling

these laterals downward in model "θ_{45}," would in theory widen the influence zone laterally as force chains will form perpendicular to the laterals. As a response, the load would be distributed to a larger volume of soil particles. In the case of "θ_{135}," force chains perpendicular to the laterals will be growing toward the main vertical pile, which would reduce the volume of the influence and resulting pullout resistance.

3.6 Effects of laterals' cross section on pullout resistance

For the various laterals' cross sections, two groups are compared: those with a similar cross-sectional area as the reference model "S_o" (i.e., "S_l" and "S_") and those with half this area (i.e., "S_n" and "S_u") (Fig. 9). For the former, laterals' cross sections with higher Z projection areas ("S_") were expected to increase pullout resistance due to higher bearing areas. Since all laterals were placed at the same depth, higher Z projection area also meant higher volume of soil directly above them. The vertical ellipse cross section "S_l" results in higher Fmax, but the horizontal one "S_" leads to higher work and displacement needed to reach Fmax. The circular cross section led to higher stiffness and lower softening. We have seen in previous sets that bearing area is usually positively correlated with Fmax, which contradicts the results in this set. Independent of the cross-sectional shape, the width of the obstacle in the direction of at the velocity is the driving factor in drag force of obstacle in granular media [42]. The displacement at Fmax seems to partly depend on the flexibility of the model's material properties. The low diameter of the laterals (i.e., 0.40 cm) and the resin used to 3D print them makes them semiflexible as indicated in the calculated deflection data. The deflection of laterals reduces their Z projection area. The variety in cross section also highly impacts their flexibility. For instance, a lateral with a cross section shaped as an ellipse with the larger radius aligned with the loading direction has a lower flexibility compared to an ellipse with the thicker radius perpendicular to the load. This observation is likely related to the difference in moments of inertia for each model: 5.80 mm^4 for "S_"; 6.28 mm^4 for "S_n" and "S_u"; 12.57 mm^4 for "S_o"; and 28.63 mm^4 for "S_l." Laterals with lower moments of inertia (i.e., smaller radius aligned with loading direction) will bend more before reaching peak force. The deflection of the laterals' tip at the maximum force was calculated for each model based on their cross-sectional moments of inertia (Table 1). The deflection of laterals was 0.79 mm (∼ 1.5 particle diameters) for "S_" and 2.95 mm (∼ 6 particle diameters) for "S_l."

For the semicircle rounded on the upper portion of the lateral ("S_n") and the circular cross sections ("S_o"), Fmax and displacement at Fmax are almost identical, showing that the jammed state only depends on the shape of the bearing surface. This similarity also suggests that laterals' deflection has a negligeable effect on pullout resistance. In comparison, when the upper portion of the laterals is flat ("S_u"), a similar Fmax is reached, but over a shorter distance. Although the projected bearing area (i.e., obstacles'

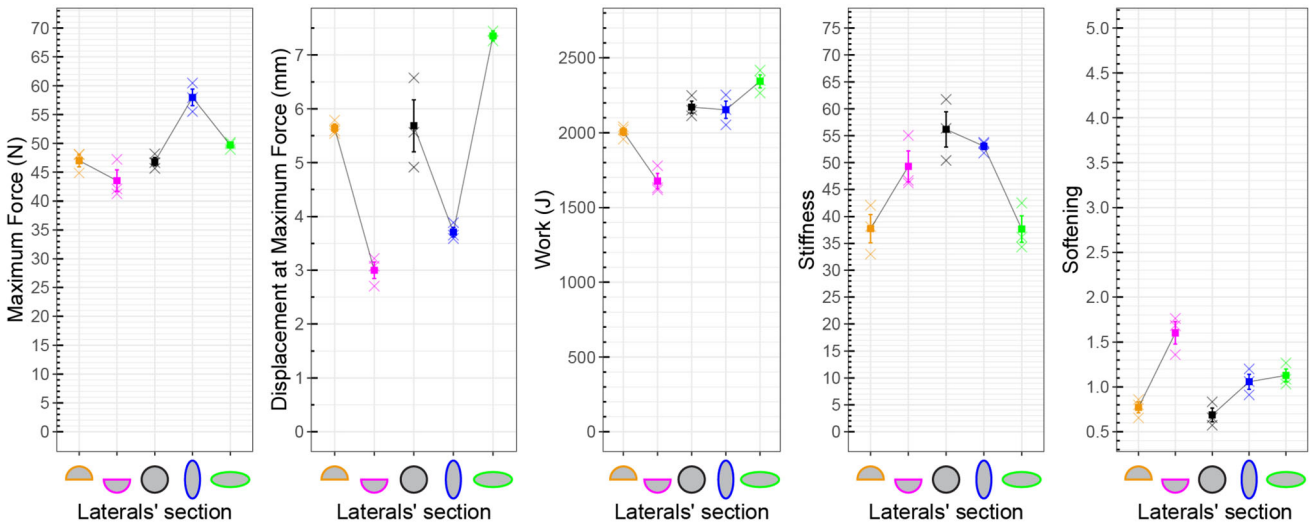

Fig. 9 Effects of the cross sections of the laterals on the maximum force, displacement at maximum force, work, stiffness and softening. Two groups are separated depending on their laterals' cross-sectional area. Laterals from the first group of models have half the cross-sectional area of those from the other group. The first group is composed of semicircle cross sections with the flat part facing downward ("S_n" in red) or upward ("S_u" in purple). The cross sections of the laterals from the second group are a circle ("S_o" in black), an ellipse with the larger radius vertical (i.e., parallel to the loading direction ("S_l" in blue)) or an ellipse with the larger radius horizontal (i.e., perpendicular to the loading direction ("S_" in green)) (color figure online)

width) of both "S_n" and "S_u" are the same, the effective bearing area of "S_n" is larger by a factor of 0.5π. These first responses before Fmax make sense in the context of the non-flowing, jammed state. In the flowing (i.e., unjammed) state after Fmax, the model with the flat surface facing upward was expected to have a higher pullout resistance than those facing downward, as a blunt body faces more resistance than a more streamlined body when pushed through a flowing medium. However, as demonstrated by Kyburz et al. [42], the size of the influence zone created by models with a curved and a flat front are similar and proportional to the obstacles' width (i.e., projected bearing area). In our pullout experiments, work is quantified to include both loading and failure of the jammed state. Having the flat portion facing upward ("S_u") led to significantly lower work compared to the other models of this trait indicates that its initial brittle response is followed by lower resistance to flow. The stiffness and softening were lower for "S_n" compared to ("S_u"). In that light, we may interpret the flat portion facing upward (i.e., acting as the bearing area) as serving to initially lock the soil grains in place. Once the system unjams, this flat surface may reduce the pullout resistance, as the corners focus stresses and disrupt force chains ahead of its motion. When the rounded part pushes through the granular media, transient force chains may more readily develop radially and more homogenously, leading to soil compaction ahead of the lateral and higher load resisted throughout pullout.

3.7 Cross-trait assessment

Since the models were parametrically built with similar features, further comparison can be performed between models of different sets (i.e., root traits). For instance, models "N_{2r}" and "B_6" have the exact same volume, surface area, Z projection area and bearing area. When compared, the placement of the six laterals at one node increases Fmax as they were placed deeper, with a total of 94.04 cm^3 of soil directly above them compared to 73.42 cm^3 for "N_{2r}" and also formed a larger bearing area at the same location in the granular media. A larger bearing area at the same depth leads to a higher possibility of arches forming between laterals and resulting in a jammed state. Inversely, this characteristic results in a lower displacement required to reach Fmax. The higher work done by the model with six laterals at the same node could result from the reasons explained in the paragraph comparing models with different number of nodes. Having an upper node unjams the upper part of the soil media. The upper node is also closer to the soil surface which decreases the overall force resisted by the model. Laterals closer to the soil surface also come out of the granular media before laterals of the lower node.

3.8 Translation of test results toward foundation systems

The foundation systems which are governed by the pullout vertical axial loads (e.g., anchors, transmission towers and offshore platforms) should support a high Fmax with low displacement at Fmax (i.e., high stiffness) and retain the load for as long as possible. Fmax refers to the maximum load resisted by the soil/structure combination. Displacement at Fmax relates to the movement of the structure before reaching the maximum resistance. Higher displacement is considered detrimental, as successive loading cycles will move the granular particles and loosen the soil media. Softening relates to the sudden decrease in the force withstood after peak force. An architectural structure should not collapse abruptly upon failure. The extra time can be vital to ensure the safety of the users and the applications of potential maintenance procedures. Thus, foundation systems should be designed with softening values as low as possible (i.e., high force maintained after Fmax). When looking at the entire pullout test, work shows how much energy is taken by the overall system. As a result, higher work means that the system resisted more force throughout the test. Consequently, all five characteristics give valuable insight into the structure's performance and should be analyzed in studies similar to the one presented here.

To show the contribution of laterals branches when added to a straight vertical pile foundation, the maximum force and stiffness for each model were normalized (Fig. 10). The maximum force resisted during the test was divided by the embedded volume of the model tested and then normalized with the result of the straight foundation pile. The same procedure was conducted to obtain the normalized stiffness. Out of the model properties analyzed, these results were divided by the volume of each model as it could directly correspond to the amount of material used to build these foundation systems. All branched models show a higher normalized maximum force than the unbranched model "X_0." Models "B_1" and "θ_{135}" only slightly increased it, while "$L_{6.75}$" and "S_l" doubled it. For the normalized stiffness, model "B_1" was significantly lower than the unbranched model "X_0" while four models ("X_x," "$L_{2.25}$," "B_6" and "θ_{135}") resulted in around 50% higher normalized stiffness. As seen throughout this work, it is necessary to analyze the test results through different variables. For example, model "θ_{135}" showed a normalized Fmax similar to the unbranched model, but a significantly higher normalized stiffness. Therefore, different models of branched foundation systems can be designed depending on the building requirements and soil mechanics phenomena at play.

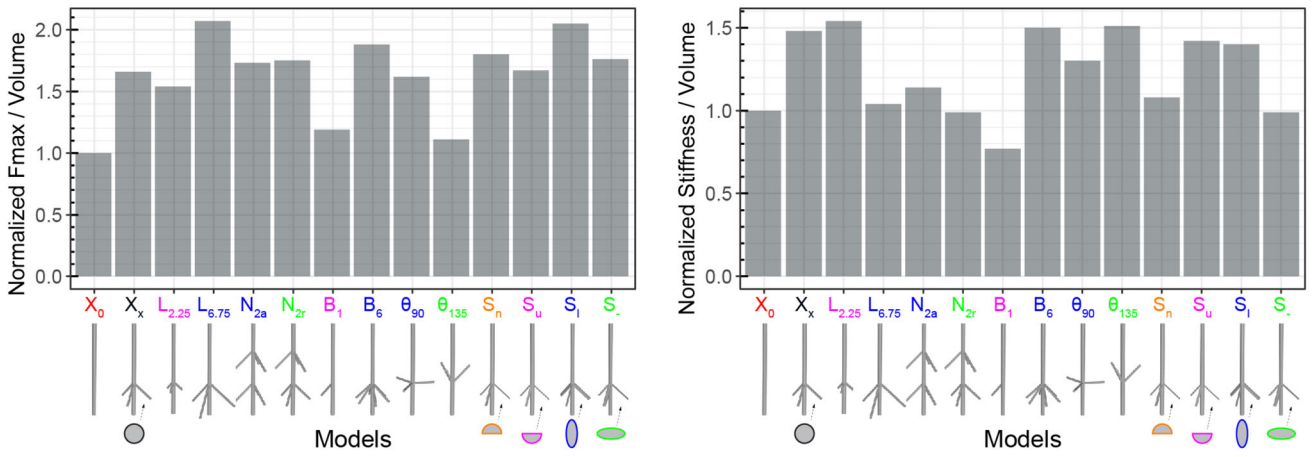

(a) (b)

Fig. 10 Maximum force (**a**), or stiffness (**b**) divided by the volume, and normalized with the unbranched model "X_0" in red. The control model is labeled as "X_x" and shown in black (color figure online)

4 Conclusion

This study explored the effect of root traits (i.e., length of laterals, number of nodes, number of laterals, branching angle and section of laterals) on the pullout resistance of branched root-inspired models. While some trends were observed between crude model properties (i.e., volume, surface area and Z projection area) and specific test results, they were not enough to characterize the differences in performance between models. In the results of the pullout tests, two main states with different behaviors were observed: initial deformations of the jammed state before flow (characterized by Fmax, displacement at Fmax and the effective stiffness); and its response after yielding, once the soil begins to rearrange (characterized by softening and work). Overall trends were observed across root traits for each test result analyzed. An increase in bearing area results in a higher maximum force resisted. Lower material flexibility and higher bearing area at the same location of the granular media (e.g., addition of laterals at one node) lead to a lower displacement at peak force reached. The presence of model parts at multiple depths (e.g., models with two nodes) disturbs and weakens the soil media during the test, therefore promoting flow and decreasing overall work to pull out. Yet, these trends did not apply to comparison between all models. Separate in-depth analyses of each root trait were therefore conducted to show their significant effects on pullout resistance. While some results were expected (e.g., longer laterals leading the higher performance), unexpected ones were observed and discussed, such as angling the laterals upward resulted in lower overall performance; adding a second node or having 6 laterals (instead to 3) increased maximum force resisted, but lowered work; laterals with vertical ellipses as cross sections led to higher peak force than horizontally shaped ones. From such results, the morphology of branched foundation systems can be tuned based on desired pullout response. These observations were obtained from sets of 4 to 5 models for each root trait analyzed and therefore have explored only a limited portion of the parameter space. Overall, trends observed in this study enhance our understanding of the effect of various morphological traits on pullout resistance and their potential for root-inspired anchorage. To go further, morphological data from real root systems pertaining to the root traits of interest can be transferred to the design of root-inspired foundation systems. In addition to these morphological traits, inspiration from other biological strategies which could be combined into their design include anisotropic surface roughness researched in snakes [55], semiflexibility of roots [49] and underground penetrating robots [11, 18, 56, 63, 71].

Acknowledgements The authors would like to thank Blake Bowser for his help with the pullout tests and characterization of sand particle size, Sina Nassiri for his assistance during the sand shear test, Julian Tao for his valuable feedback on the experimental setup, Peter Niewiarowski for his guidance in the early steps, both Henry Astley and Randall Mitchell for their support in the data/statistical analysis, and the reviewers for their insightful comments.

Data availability Data are available upon request to the authors.

References

1. Abe K, Ziemer RR (1991) Effect of tree roots on a shear zone: modeling reinforced shear stress. Can J For Res 21:1012–1019. https://doi.org/10.1139/x91-139

2. Alaoui A, Rogger M, Peth S, Blöschl G (2018) Does soil compaction increase floods? A review. J Hydrol 557:631–642
3. Albert R, Pfeifer MA, Barabási A-L, Schiffer P (1999) Slow drag in a granular medium. Phys Rev Lett 82:205–208. https://doi.org/10.1103/PhysRevLett.82.205
4. De Baets S, Poesen J, Gyssels G, Knapen A (2006) Effects of grass roots on the erodibility of topsoils during concentrated flow. Geomorphology 76:54–67. https://doi.org/10.1016/j.geomorph.2005.10.002
5. Bailey PHJ, Currey JD, Fitter AH (2002) The role of root system architecture and root hairs in promoting anchorage against uprooting forces in *Allium cepa* and root mutants of *Arabidopsis thaliana*. J Exp Bot 53:333–340. https://doi.org/10.1093/jexbot/53.367.333
6. Behringer RP, Chakraborty B (2019) The physics of jamming for granular materials: a review. Reports Prog Phys 82:012601. https://doi.org/10.1088/1361-6633/aadc3c
7. Bouma TJ, Nielsen KL, Van Hal H, Koutstaal B (2001) Root system topology and diameter distribution of species. Funct Ecol 15:360–369. https://doi.org/10.1046/j.1365-2435.2001.00523.x
8. Broms BB (1964) Lateral resistance of piles in cohesive soils. J Soil Mech Found Div 90:27–63. https://doi.org/10.1061/JSFEAQ.0000611
9. Burrall M, DeJong JT, Martinez A, Wilson DW (2020) Vertical pullout tests of orchard trees for bio-inspired engineering of anchorage and foundation systems. Bioinspir Biomim 16:016009. https://doi.org/10.1088/1748-3190/abb414
10. Burrall M, DeJong JT, Martinez A, Wilson DW, Huang L (2020) Bio-inspiration through tree root pullout tests for innovative anchorage design. In: Geo-congress 2020. American Society of Civil Engineers (ASCE), 233–242
11. Calderón AA, Ugalde JC, Chang L, Cristóbal Zagal J, Pérez-Arancibia NO (2019) An earthworm-inspired soft robot with perceptive artificial skin. Bioinspir Biomim 14:056012. https://doi.org/10.1088/1748-3190/ab1440
12. Coutts MP (1983) Root architecture and tree stability. Plant Soil 188:171–188
13. Danjon F, Barker DH, Drexhage M, Stokes A (2008) Using three-dimensional plant root architecture in models of shallow-slope stability. Ann Bot 101:1281–1293. https://doi.org/10.1093/aob/mcm199
14. Danjon F, Fourcaud T, Bert D (2005) Root architecture and wind-firmness of mature *Pinus pinaster*. New Phytol 168:387–400. https://doi.org/10.1111/j.1469-8137.2005.01497.x
15. Das BM (2007) Principles of foundation engineering, 6th edn. Cengage Learning Inc, Florence
16. DeJong JT, Burrall M, Wilson DW, Frost JD (2017) A bio-inspired perspective for geotechnical engineering innovation. In: Geotechnical frontiers 2017. American Society of Civil Engineers (ASCE), Orlando, 862–870
17. Doreau-Malioche J, Galvis-Castro A, Tovar-Valencia R, Viggiani G, Combe G, Prezzi M, Salgado R (2019) Characterising processes at sand-pile interface using digital image analysis and X-ray CT. Géotechnique Lett 9:254–262. https://doi.org/10.1680/jgele.18.00232
18. Del Dottore E, Mondini A, Sadeghi A, Mattoli V, Mazzolai B (2018) An efficient soil penetration strategy for explorative robots inspired by plant root circumnutation movements. Bioinspir Biomim 13:015003. https://doi.org/10.1088/1748-3190/AA9998
19. Duckett N (2014) Development of improved predictive tools for mechanical soil root interaction. University of Dundee
20. Dupuy L, Fourcaud T, Lac P, Stokes A (2007) A generic 3D finite element model of tree anchorage integrating soil mechanics and real root system architecture. Am J Bot 94:1506–1514. https://doi.org/10.3732/ajb.94.9.1506
21. Dupuy L, Fourcaud T, Stokes A (2005) A numerical investigation into factors affecting the anchorage of roots in tension. Eur J Soil Sci 56:319–327. https://doi.org/10.1111/j.1365-2389.2004.00666.x
22. Dupuy L, Fourcaud T, Stokes A (2005) A numerical investigation into the influence of soil type and root architecture on tree anchorage. In: Plant and soil. Springer, 119–134
23. Duraiappah AK, Naeem S, Agardy T, Ash NJ, Cooper HD, Diaz S, Faith DP, Mace G, McNeely JA, Mooney HA, Oteng-Yeboah AA, Pereira HM, Polasky S, Prip C, Reid W V., Samper C, Schei PJ, Scholes R, Schutyser F, Van Jaarsveld A (2005) Ecosystems and human well-being: biodiversity synthesis; a report of the millennium ecosystem assessment. World Resources Institute
24. Dyson AS, Rogno PG (2015) Pull-out capacity of tree root inspired anchors in shallow granular soils. Géotechnique Lett 4:301–305. https://doi.org/10.1680/GEOLETT.14.00061
25. Easson DL, Pickles SJ, White EM (1995) A study of the tensile force required to pull wheat roots from soil. Ann Appl Biol 127:363–373. https://doi.org/10.1111/J.1744-7348.1995.TB06680.X
26. Ennos AR (1990) The anchorage of leek seedlings: the effect of root length and soil strength. Ann Bot 65:409–416. https://doi.org/10.1093/OXFORDJOURNALS.AOB.A087951
27. Ennos AR (2000) The mechanics of root anchorage. Adv Bot Res 33:133–157. https://doi.org/10.1016/s0065-2296(00)33042-7
28. Ennos AR, Pellerin S (2000) Plant anchorage. In: Smit AL, Bengough AG, Engels C, van Noordwijk M, Pellerin S, van de Geijn SC (eds) Root methods. Springer, Berlin, Heidelberg, pp 545–565
29. Fourcaud T, Ji JN, Zhang ZQ, Stokes A (2008) Understanding the impact of root morphology on overturning mechanisms: a modelling approach. Ann Bot 101:1267–1280. https://doi.org/10.1093/aob/mcm245
30. Frost JD, Martinez A, Mallett SD, Roozbahani MM, DeJong JT (2017) Intersection of modern soil mechanics with ants and roots. In: Geotechnical special publication. American Society of Civil Engineers (ASCE), 900–909
31. Galvis-Castro AC, Tovar-Valencia RD, Salgado R, Prezzi M (2019) Effect of loading direction on the shaft resistance of jacked piles in dense sand. Géotechnique 69:16–28. https://doi.org/10.1680/jgeot.17.P.046
32. Ghestem M, Veylon G, Bernard A, Vanel Q, Stokes A (2014) Influence of plant root system morphology and architectural traits on soil shear resistance. Plant Soil 377:43–61. https://doi.org/10.1007/s11104-012-1572-1
33. Gray DH (1974) Reinforcement and stabilization of soil by vegetation. J Geotech Geoenvironmental Eng 100:695–699
34. Grimm NB, Faeth SH, Golubiewski NE, Redman CL, Wu J, Bai X, Briggs JM (2008) Global change and the ecology of cities. Science 80(319):756–760
35. Gyssels G, Poesen J, Bochet E, Li Y (2005) Impact of plant roots on the resistance of soils to erosion by water: a review. Prog Phys Geogr Earth Environ 29:189–217. https://doi.org/10.1191/0309133305pp443ra
36. Hobst L, Zaijíc J (1983) Anchoring in rock and soil, 2nd edn. Elsevier Scientific Publishing Company, Amsterdam
37. Hossain T, Rognon P (2020) Rate-dependent drag instability in granular materials. Granul Matter 22:72. https://doi.org/10.1007/s10035-020-01039-5
38. Houette T, Stachew E, Naményi C, Miesbauer JW, Gruber P (2023) Parametric algorithms to extract root traits for biology and biomimicry. In: Dortdivanlioglu H, Panagoulia E, Oh Y (eds) Divergence in architectural research: ConCave Ph.D. symposium 2022, Accessed 7–8 April 2022. Georgia Institute of Technology, Atlanta, 77–94

39. Huang S, Tao J (2020) Modeling clam-inspired burrowing in dry sand using cavity expansion theory and DEM. Acta Geotech 15:2305–2326. https://doi.org/10.1007/s11440-020-00918-8
40. Khosravi A, Martinez A, Dejong J, Wilson D (2018) Discrete element simulations of bio-inspired self-burrowing probes in sands of varying density. In: Proceedings of biomediated and bioinspired geotechnics conference (B2G) Atlanta, GA
41. Kozlowski TT, Kramer PJ, Pallardy SG (1991) The physiological ecology of woody plants. Academic Press, New York
42. Kyburz ML, Sovilla B, Gaume J, Ancey C (2022) The concept of the mobilized domain: how it can explain and predict the forces exerted by a cohesive granular avalanche on an obstacle. Granul Matter 24:45. https://doi.org/10.1007/s10035-021-01196-1
43. Liu CH, Nagel SR, Schecter DA, Coppersmith SN, Majumdar S, Narayan O, Witten TA (1995) Force fluctuations in bead packs. Science 80(269):513–515. https://doi.org/10.1126/science.269.5223.513
44. Liu J, Liu M, Zhu Z (2012) Sand deformation around an uplift plate anchor. J Geotech Geoenvironmental Eng 138:728–737. https://doi.org/10.1061/(asce)gt.1943-5606.0000633
45. Lotze HK, Lenihan HS, Bourque BJ, Bradbury RH, Cooke RG, Kay MC, Kidwell SM, Kirby MX, Peterson CH, Jackson JBC (2006) Depletion degradation, and recovery potential of estuaries and coastal seas. Science 80(312):1806–1809. https://doi.org/10.1126/science.1128035
46. Mallett SD (2019) Mechanical behavior of fibrous root-inspired anchorage systems. Georgia Institute of Technology
47. Mallett SD, Matsumura S, Frost JD (2018) Additive manufacturing and computed tomography of bio-inspired anchorage systems. Géotechnique Lett 8:219–225. https://doi.org/10.1680/JGELE.18.00090
48. Meijer GJ, Muir Wood D, Knappett JA, Bengough AG, Liang T (2019) Root branching affects the mobilisation of root-reinforcement in direct shear. In: E3S Web of Conferences 92:12010. https://doi.org/10.1051/E3SCONF/20199212010
49. Mickovski SB, Bengough AG, Bransby MF, Davies MCR, Hallett PD, Sonnenberg R (2007) Material stiffness, branching pattern and soil matric potential affect the pullout resistance of model root systems. Eur J Soil Sci 58:1471–1481. https://doi.org/10.1111/J.1365-2389.2007.00953.X
50. Mickovski SB, Bransby MF, Bengough AG, Davies MCR, Hallett PD (2010) Resistance of simple plant root systems to uplift loads. Can Geotech J 47:78–95. https://doi.org/10.1139/T09-076
51. Mueth DM, Jaeger HM, Nagel SR (1998) Force distribution in a granular medium. Phys Rev E 57:3164–3169. https://doi.org/10.1103/PhysRevE.57.3164
52. Nicoll BC, Dunn AJ (2000) The effects of wind speed and direction on radial growth of structural roots. In: Stokes A (ed) The supporting roots of trees and woody plants: form, function and physiology. Springer, Netherlands, pp 219–225
53. Nicoll BC, Gardiner BA, Peace AJ (2008) Improvements in anchorage provided by the acclimation of forest trees to wind stress. Forestry 81:389–398. https://doi.org/10.1093/forestry/cpn021
54. Nicoll BC, Ray D (1996) Adaptive growth of tree root systems in response to wind action and site conditions. Tree Physiol 16:891–898. https://doi.org/10.1093/treephys/16.11-12.891
55. O'Hara KB, Martinez A (2020) Monotonic and cyclic frictional resistance directionality in snakeskin-inspired surfaces and piles. J Geotech Geoenvironmental Eng 146:04020116. https://doi.org/10.1061/(ASCE)GT.1943-5606.0002368
56. Ozkan-Aydin Y, Murray-Cooper M, Aydin E, McCaskey EN, Naclerio N, Hawkes EW, Goldman DI (2019) Nutation AIDS heterogeneous substrate exploration in a robophysical root. In: RoboSoft 2019-2019 IEEE international conference on soft robotics. Institute of Electrical and Electronics Engineers Inc., pp 172–177
57. Pandey BK, Huang G, Bhosale R, Hartman S, Sturrock CJ, Jose L, Martin OC, Karady M, Voesenek LACJ, Ljung K, Lynch JP, Brown KM, Whalley WR, Mooney SJ, Zhang D, Bennett MJ (2021) Plant roots sense soil compaction through restricted ethylene diffusion. Science 80(371):276–280. https://doi.org/10.1126/SCIENCE.ABF3013/SUPPL_FILE/ABF3013_REPRODUCIBILITY-CHECKLIST.PDF
58. Potocka I, Szymanowska-Pulka J (2018) Morphological responses of plant roots to mechanical stress. Ann Bot 122:723. https://doi.org/10.1093/AOB/MCY010
59. Qian F, Lee D, Nikolich G, Koditschek D, Jerolmack D (2019) Rapid in situ characterization of soil erodibility with a field deployable robot. J Geophys Res Earth Surf 124:1261–1280. https://doi.org/10.1029/2018JF004887
60. Read J, Stokes A (2006) Plant biomechanics in an ecological context. Am J Bot 93:1546–1565. https://doi.org/10.3732/AJB.93.10.1546
61. Reubens B, Poesen J, Danjon F, Geudens G, Muys B (2007) The role of fine and coarse roots in shallow slope stability and soil erosion control with a focus on root system architecture: a review. Trees - Struct Funct 21:385–402. https://doi.org/10.1007/s00468-007-0132-4
62. Rogers ED, Monaenkova D, Mijar M, Nori A, Goldman DI, Benfey PN (2016) X-ray computed tomography reveals the response of root system architecture to soil texture. Plant Physiol 171:2028–2040. https://doi.org/10.1104/pp.16.00397
63. Sadeghi A, Mondini A, Mazzolai B (2017) Toward self-growing soft robots inspired by plant roots and based on additive manufacturing technologies. Soft Robot 4:211–223. https://doi.org/10.1089/soro.2016.0080
64. Schwarz M, Cohen D, Or D (2010) Root-soil mechanical interactions during pullout and failure of root bundles. J Geophys Res Earth Surf. https://doi.org/10.1029/2009JF001603
65. Schwarz M, Cohen D, Or D (2011) Pullout tests of root analogs and natural root bundles in soil: experiments and modeling. J Geophys Res Earth Surf. https://doi.org/10.1029/2010JF001753
66. Sperl M (2006) Experiments on corn pressure in silo cells-translation and comment of Janssen's paper from 1895. Granul Matter 8:59–65. https://doi.org/10.1007/s10035-005-0224-z
67. Stachew E, Houette T, Gruber P (2021) Root systems research for bioinspired resilient design: a concept framework for foundation and coastal engineering. Front Robot AI 8:109. https://doi.org/10.3389/frobt.2021.548444
68. Stokes A, Atger C, Bengough AG, Fourcaud T, Sidle RC (2009) Desirable plant root traits for protecting natural and engineered slopes against landslides. Plant Soil 324:1–30. https://doi.org/10.1007/s11104-009-0159-y
69. Stokes A, Ball J, Fitter AH, Brain P, Coutts MP (1996) An experimental investigation of the resistance of model root systems to uprooting. Ann Bot 78:415–421. https://doi.org/10.1006/ANBO.1996.0137
70. Tamasi E, Stokes A, Lasserre B, Danjon F, Berthier S, Fourcaud T, Chiatante D (2005) Influence of wind loading on root system development and architecture in oak (*Quercus robur* L.) seedlings. Trees 19:374–384. https://doi.org/10.1007/s00468-004-0396-x
71. Tao JJ, Huang S, Tang Y (2020) SBOR: a minimalistic soft self-burrowing-out robot inspired by razor clams. Bioinspir Biomim 15:55003. https://doi.org/10.1088/1748-3190/ab8754
72. Tisdall JM, Cockroft B, Uren NC (1978) The stability of soil aggregates as affected by organic materials, microbial activity and physical disruption. Aust J Soil Res 16:9–17. https://doi.org/10.1071/SR9780009

73. Vego I, Ceccato F, Simonini P, Frost JD, Mallett SD, Cola S (2021) Numerical investigation of failure mechanism during pullout of root inspired anchorages. In: Barla M, Di Donna A, Sterpi D (eds) Challenges and innovations in geomechanics. Springer International Publishing, Cham, pp 111–118
74. Waldron LJ (1977) The shear resistance of root-permeated homogeneous and stratified soil. Soil Sci Soc Am J 41:843–849. https://doi.org/10.2136/sssaj1977.03615995004100050005x
75. Watson GW, Hewitt AM, Custic M, Lo M (2014) The management of tree root systems in urban and suburban settings: a review of soil influence on root growth. Arboric Urban For 40:193–217
76. Wu TH, McOmber RM, Erb RT, Beal PE (1988) Study of soil-root interaction. J Geotech Eng 114:1351–1375. https://doi.org/10.1061/(ASCE)0733-9410(1988)114:12(1351)
77. Yang JL, Zhang GL (2011) Water infiltration in urban soils and its effects on the quantity and quality of runoff. J Soils Sediments 11:751–761. https://doi.org/10.1007/s11368-011-0356-1